図7　secondary stabilizerとしての内側半月板の機能

ⓐ：前十字靱帯が正常な場合は内側半月板に負荷がかかる前に前十字靱帯によって前方制動が起こる。
ⓑ：前十字靱帯損傷時には内側半月板が楔状に大腿脛骨関節に介在し前方移動を抑制する。

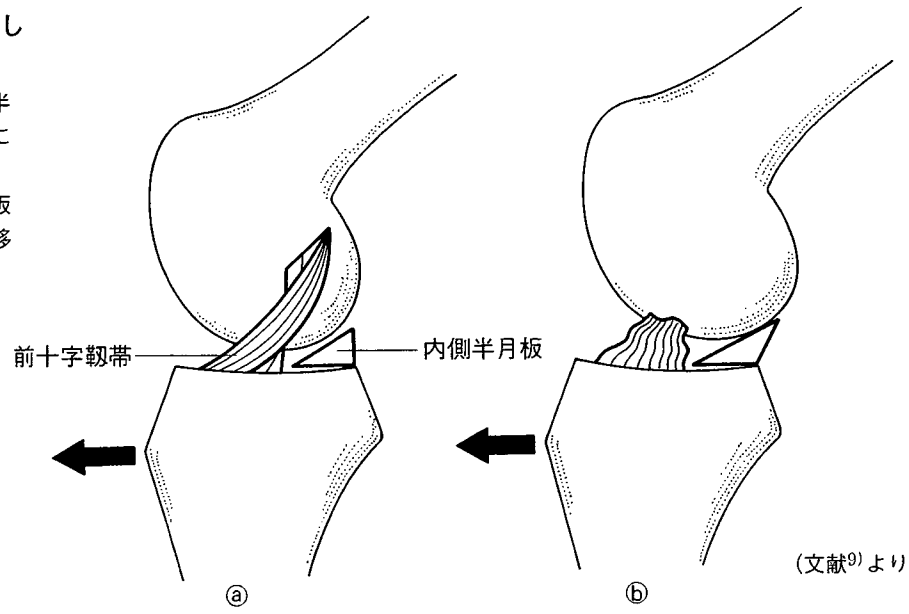

(文献[9]より)

が大腿骨と脛骨の間に楔状に介在して脛骨の前方移動を抑制するために生じる現象であるが(**図7**)，もともと膝屈伸に伴う前後移動量が大きい外側半月板では同様の現象はみられない。また，内側半月板切除の影響は膝屈曲位でより大きいことから，半月板のsecondary stabilizerとしての膝関節安定性への関与は，後方関節包なども含めた部分的なものと考えられる。

また，近年の研究によれば半月板は膝関節の内外側の安定性や回旋運動にも影響を与えていることが報告されているが，いまだ明らかになっていない点も多い[11]。今後，dynamic MRIなど*in vivo*での動的な解析が進むことにより，半月板の機能に関する新しい知見が得られることが期待される。

◆文　献◆

1)黒坂昌弘：半月損傷. 膝のスポーツ傷害. 医学書院, 東京, 1995, p35-67.
2)滝　正徳, 木村雅史：半月板のバイオメカニクス. 最新整形外科学体系17, 膝関節・大腿. 中山書店, 東京, 2006, p310-315.
3)Fairbank TL：Knee joint changes after menisectomy. J Bone Joint Surg, 30-B：664-670, 1948.
4)Vedi V, Williams A, Tennant SJ, et al：Meniscal movement. J Bone Joint Surg, 81-B：37-41, 1999.
5)Ahmed AM, Burke DL：*In-vitro* measurement of static pressure distribution in synovial joints－Part 1：Tibial surface of the knee. J Biomech Eng, 105：216-225, 1983.
6)Kurosawa H, Fukubayashi T, Nakajima H：Load-bearing mode of the knee joint：physical behavior of the knee joint with or without menisci. Clin Orthop Relat Res, 149：283-290, 1980.
7)Fukubayashi T, Kurosawa H：The contact area and pressure distribution pattern of the knee. A study of normal and osteoarthrotic knee joints. Acta Orthop Scand, 51：871-879, 1980.
8)Jones RS, Keene GCR, Learmonth DJA, et al：Direct measurement of hoop strains in the intact and torn human medial meniscus. Clin Biomech, 11：295-300, 1996.
9)Levy IM, Torzilli PA, Warren RF：The effect of medial meniscectomy on anterior-posterior motion of the knee. J Bone Joint Surg, 64-A：883-888, 1982.
10)Levy IM, Torzilli PA, Gould JD, et al：The effect of lateral meniscectomy on motion of the knee. J Bone Joint Surg, 71-A：401-406, 1989.
11)寺田宏平, 竹中　慎, 池内　健ほか：関節荷重下での膝半月板のバイオメカニクス. 日本臨床バイオメカニクス学会誌, 23：185-190, 2002.

装具の基本となるバイオメカニクスとウィンタースポーツにおける装具

変形性膝関節症用装具のバイオメカニクス －機能的装具効果の検討事例－

西野勝敏[*1]，長崎浩爾[*2]，大森　豪[*3]
古賀良生[*4]，田中正栄[*1]，山本智章[*5]

はじめに

変形性膝関節症(膝OA)は，中高齢者の運動器疾患の１つである．国の重点施策である「活力ある高齢社会の実現」には，自立した生活を送るために運動器の健康を維持する必要があり，本症の発症因子の解明と適切な対応が求められている．膝OAの発症因子について渡辺ら[1]は21年間の膝OAの疫学調査から歩行立脚初期にみられるスラスト(**図-1**)が関与し，さらに大腿脛骨角増加による膝内反変形および膝関節屈曲拘縮による伸展制限との関連性を報告している．運動学的にはスラストによる急激な膝内反は膝関節内側への荷重負荷を増加し，膝OAの発症と進行に影響すると考えられるが，近年では膝OAの機能的装具による動的矯正機能としてのスラスト抑制への効果が注目されている．

膝OAの装具には足底板やサポーター式軟性装具，継ぎ手や支柱を用いた機能的装具(膝装具)があり，その効果についてさまざまな研究がなされている[2]．中でも膝装具については非常に多くの機種が使用されている．膝装具の効果については，疼痛改善など臨床成績の向上についての報告[3,4]が多くみられるが，運動学的・動力学的観点から詳細に研究した報告は少ない．運動学的・動力学的効果の研究で最も多くみられるのがビデオカメラの映像やセンサーなどの検出器具を用いた分析[5]である．しかし，これらは大腿骨と脛骨で構成される膝関節運動を直接評価したものではない．また，X線を用いて骨の動態変化を直接検討している報告[6,7]も散見されているが，測定環境から運動範囲や荷重条件に制限があり，生理的な状態を反映できていない．

われわれも膝装具の効果について詳細を把握しようと運動学的・動力学的観点でさまざまな分析を試みている．本稿では，その研究結果を紹介し今後の課題について述べる．

膝装具効果の検討

1．三次元下肢アライメントへの影響[8]

a．方　法

膝装具による下肢アライメントへの影響を検討するために，KneeCAS (株式会社 LEXI) を用いて下肢アライメントの三次元的変化を**図-2**の手順で解析した．まず立位荷重状態の下肢を正面と60度斜角の２方向からX線撮影する．次にX線像をコンピュータに取り込み，骨の特徴点をデジタイズしたデータを基に骨モデルをX線像へ重ね合わせをして骨の三次元情報を得る．最後に**図-3**で示した下肢アライメントの評価パラメータを算出する．パラメータは膝関節の三次元的アライメントとして大腿脛骨角，立位屈曲角，脛骨回旋角を

*1 新潟県健康づくり・スポーツ医科学センター
*2 北陸電力科学研究所
*3 新潟大学超域研究機構
*4 [illegible]病院
*5 [illegible]リテーション病院

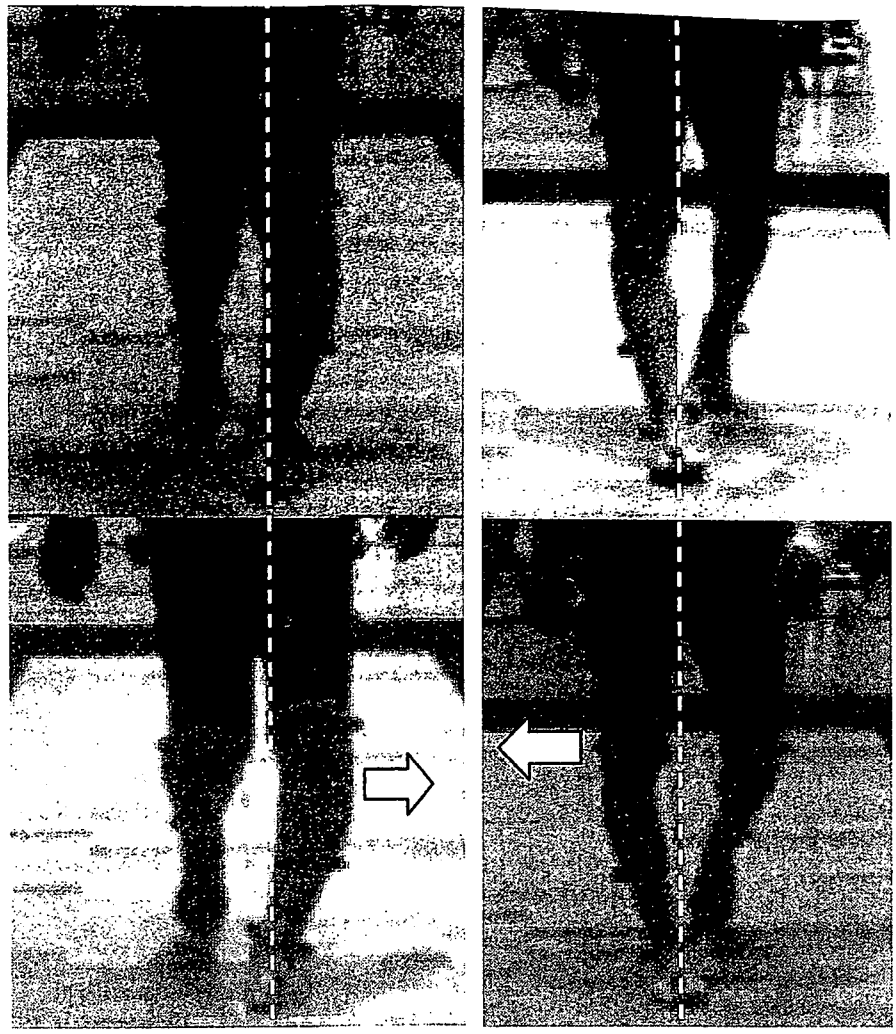

図-1　スラストの代表例
左図が女性右膝，右が男性左膝．

求めた．さらに，大腿骨頭中心と足関節中心とを結んだ線を下肢荷重線とし，この線の脛骨関節面への通過点(下肢荷重線通過点)や関節裂隙角など評価した．

b．対　象

膝装具は，外反矯正を目的とした内側ヒンジ型(**図-4a**)と外側ヒンジ型(**図-4b**)の異なる機構の２種を用いた．被験者は全て内反膝OAの女性で，内側ヒンジ型装着群が５名(平均70.6歳)，外側ヒンジ型装着群が７名(平均68.3歳)であった．

c．結果と考察

表-1に膝装具装着による下肢アライメントの評価パラメータの変化を示す．２種とも膝装具装着により，大腿脛骨角の外反，脛骨回旋角の外旋，関節裂隙角の外反がみられ，ほぼ全てのパラメータが膝OAを矯正する方向へ変化していた．下肢荷重線通過点も膝装具によって外側へ位置したことから，膝OA特有の内側型荷重が軽減されている可能性が示された．この結果から，膝装具は下肢アライメントの異常環境を矯正する作用があることがわかったが，機構の違いによる作用機序までは検討できなかった．

2．歩行中の膝運動への影響[9)]

a．方　法

動的環境での効果を検討するため，膝装具を用いた歩行を分析した．膝OAの歩行分析にはMotion capture system[11)]や加速度センサー[12)]などを用いた報告があるが，われわれは**図-5**に示す

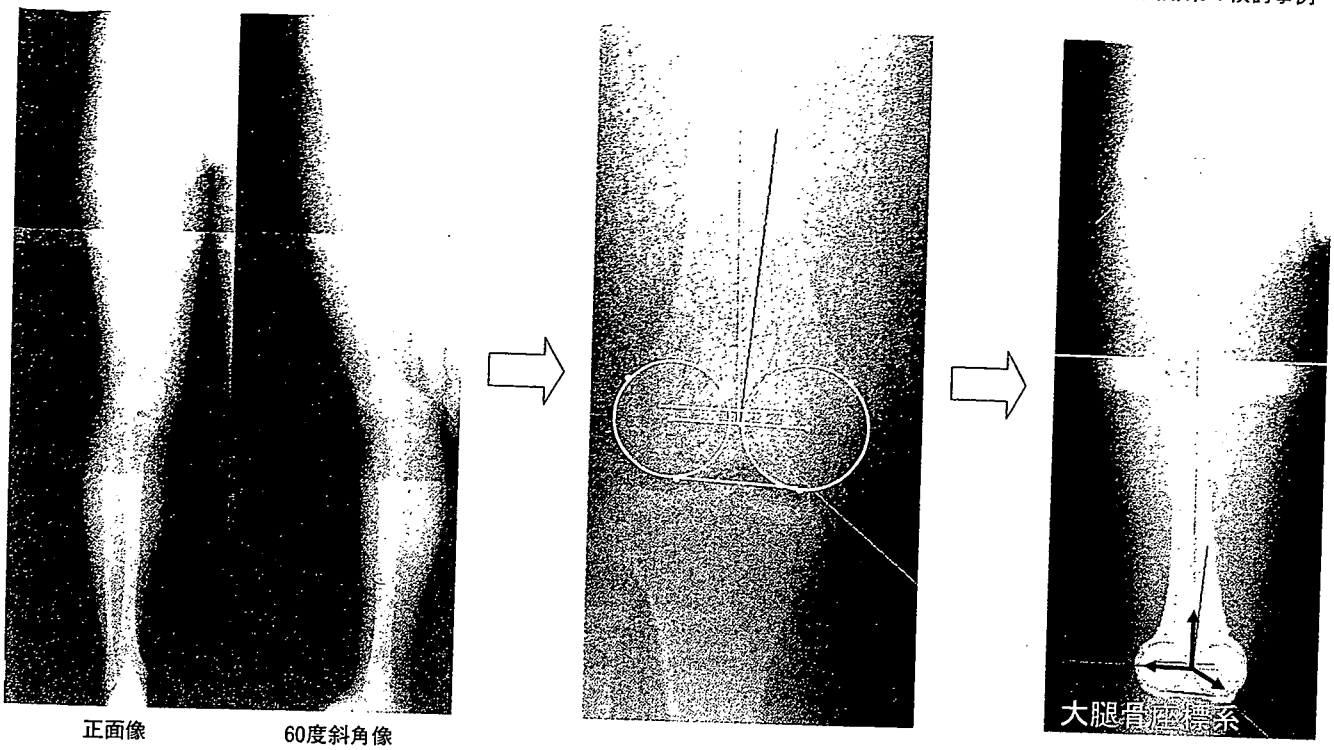

a. X線像の取り込み　b. 骨特徴点のデジタイズ　c. 骨モデルの重ね合わせ

図-2 三次元下肢アライメント解析の手順(文献８より引用)

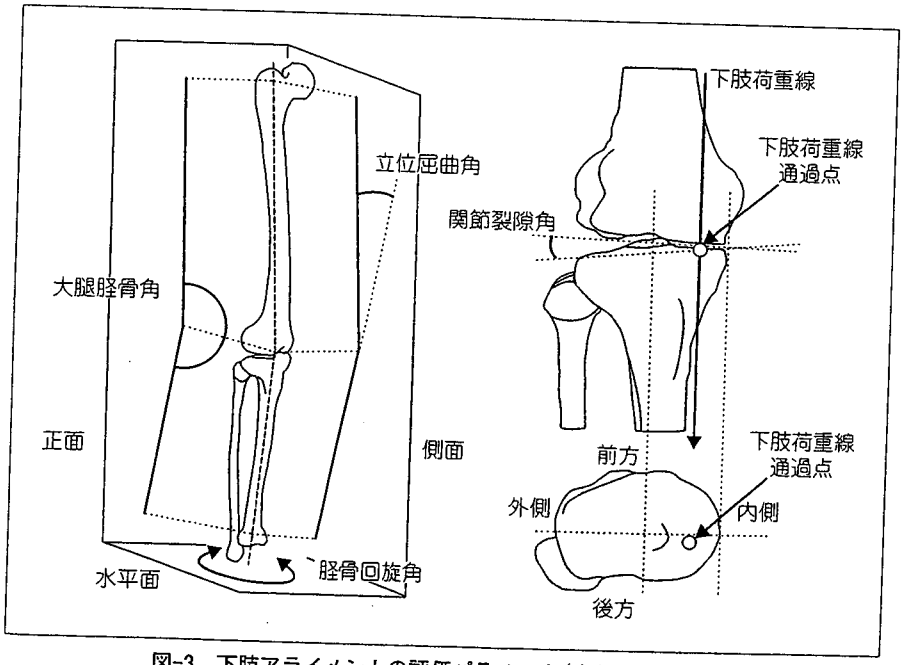

図-3 下肢アライメントの評価パラメータ(文献８より引用)

易的かつ三次元分析可能な６自由度電気角度[8~10]を用いた．この角度計を用いた先行研[10]では，膝OAの運動範囲は狭くなる傾向にり，スラストを脛骨の内反，外旋，内側移動をう三次元的な運動と定義した．そのため，動的環境下での効果を運動学的に評価するには，三次元的な手法が必要不可欠である．

b. 対　象

対象は，内反膝OAの女性７名(平均65.2歳)とした．用いた膝装具は外側ヒンジ型(図-4b)と

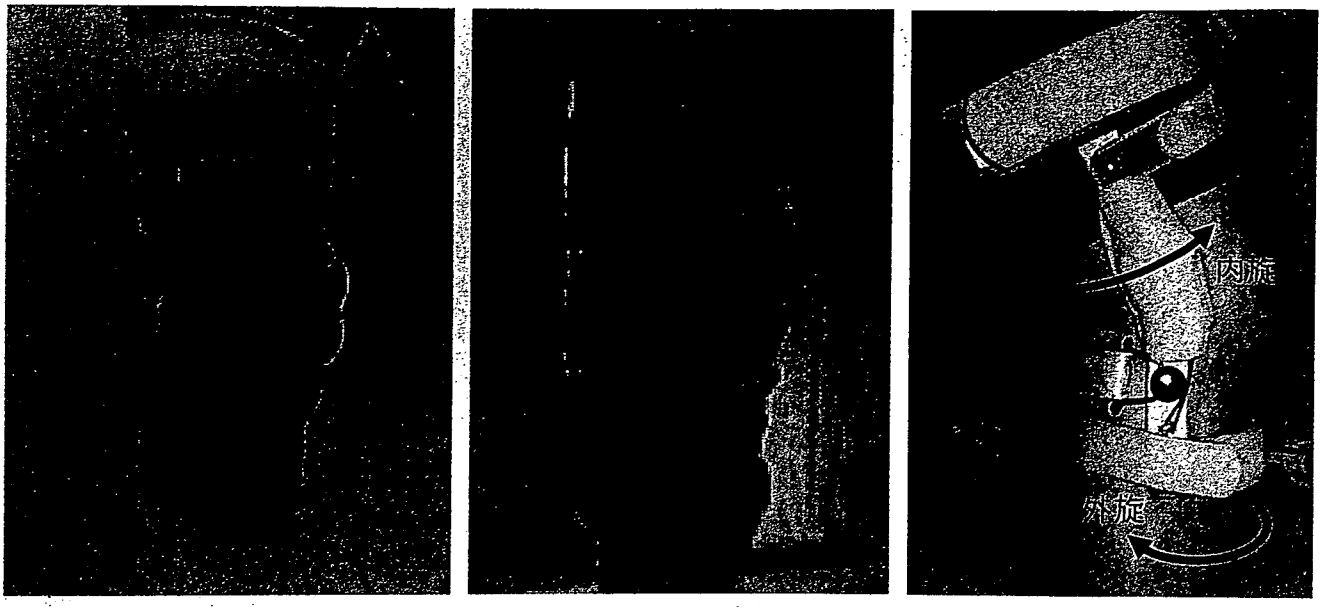

a. 内側ヒンジ型　　b. 外側ヒンジ型　　c. 回旋矯正型

図-4 膝 OA 用機能的装具

表-1 装具装着による下肢アライメントの評価パラメータの変化(文献８より引用)

評価パラメータ	内側ヒンジ型	外側ヒンジ型
大腿脛骨角[度]	外反1.0±1.6度	外反2.2±2.0度
立位屈曲角[度]	伸展4.4±2.2度	屈曲3.7±3.3度
脛骨回旋角[度]	外旋2.9±3.6度	外旋4.6±7.4度
関節裂隙角[度]	外反1.2±2.6度	外反2.1±2.3度
下肢荷重線通過点	脛骨面の外側前方	脛骨面の外側後方

し，膝装具の有無をヒンジ部の有無に置き換えて測定した．

c． 結果と考察

膝装具によって運動範囲が狭くなったが，とくに装着前にみられたスラストの特徴である立脚初期の内反が全対象で消失していた．この結果から，膝装具は静的環境のみならず動的環境下でも矯正作用があることが判明した．

3． 膝装具の作用機序の検討[13)]

a． 対象と方法

膝装具の機構の違いによる矯正への作用機序を調査するため，直接矯正を与える場所の接触圧を測定した．測定には感圧導電ゴムセンサー(イナバゴム社)を用い，膝装具が当たる皮膚表面に貼付した．用いた膝装具は，内側ヒンジ型と外側ヒンジ型の異なる機構の２種(**図-4a,b**)とした．

b． 結果と考察

測定の結果，内側ヒンジ型では大腿部の外側で高い接触圧がみられたが，外側ヒンジ型では大腿部と脛部の内側で高い接触圧がみられた(**図-6**)．これから，内側ヒンジ型はストラップの外側への引っ張りによる三点曲げで，外側ヒンジ型はヒンジの膝への押し付けによる三点曲げの外反矯正機序を有することが推察された．しかし，ストラップやヒンジによる圧力は被験者のサイズや形態に依存するため，さらなる検証が必要と考える．

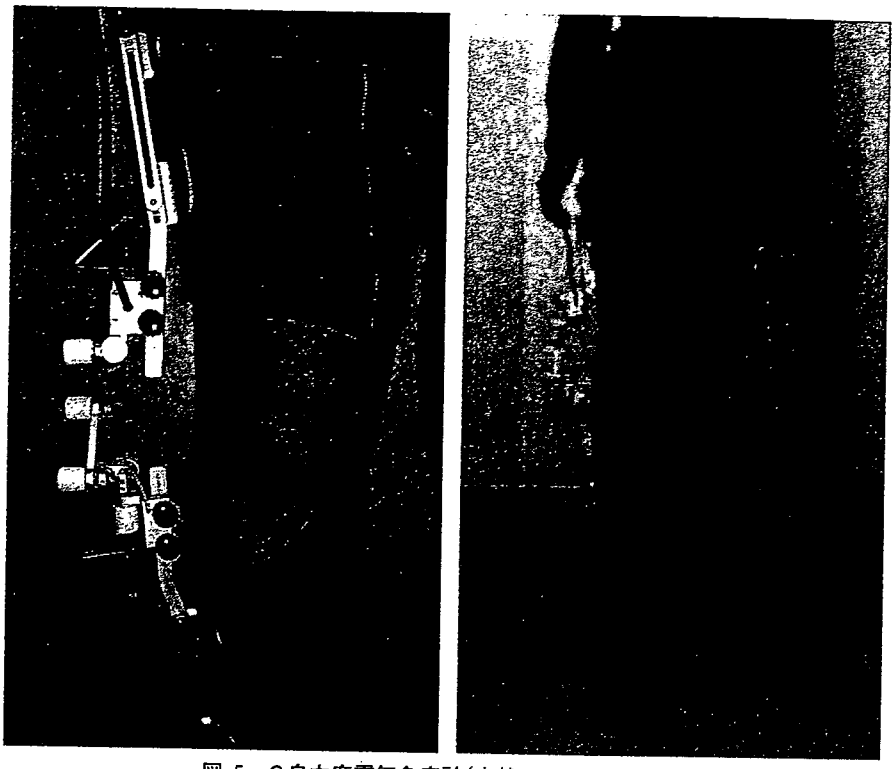

図-5　6自由度電気角度計(文献８～10より引用)

4．Motion capture system による検討

a．方　法

Motion capture system で用いる反射マーカーに硬球を埋め込み，それを下肢に貼付して２方向X線撮影する(**図-7a**)．このマーカーを貼付したまま，装具有無における歩行運動を測定した．Motion capture system は，VICON (Vicon Motion Systems 社) を用いた．

解析では１で述べた静的三次元下肢アライメント解析の他に，X線像上に投影された反射マーカーの位置と下肢アライメント解析で決定した骨座標系との位置関係を求めた(**図-7b**)．このデータと歩行運動データとを組み合わせることで歩行空間内に下肢骨を求め，大腿脛骨運動を推定した(**図-7c**)．この処理によって歩行中の床反力や下肢荷重線と下肢骨との関係や回旋運動などの三次元情報を算出することなどができる．

b．対　象

対象は，内反膝OA患者２名で，45歳男性１名と57歳女性１名とした．膝装具は，膝回旋運動を矯正することを目的とした回旋矯正型(**図-4c**)を用いた．

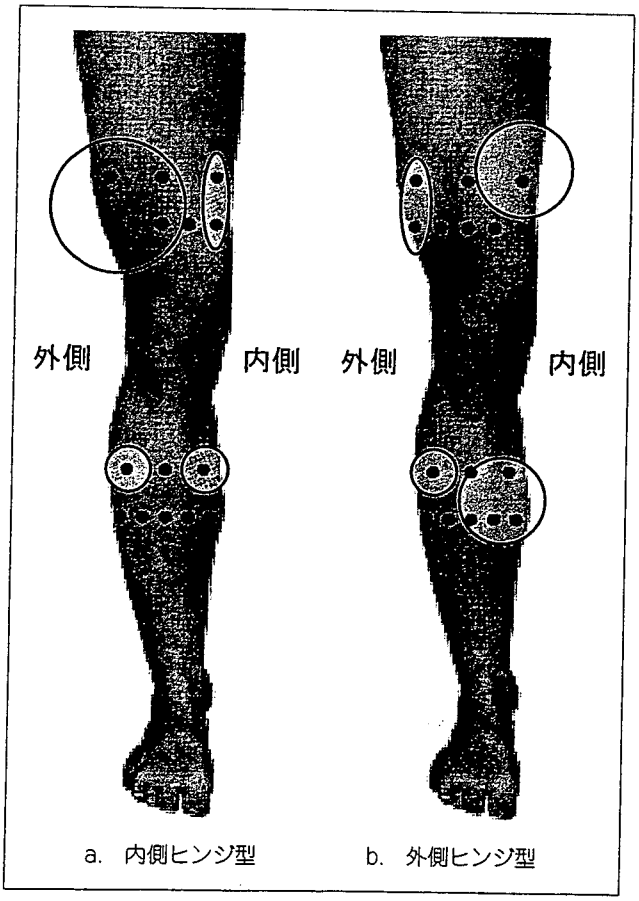

図-6　膝装具による接触圧分布(文献13を改変)
円は接触圧が生じた位置と大きさを示す．

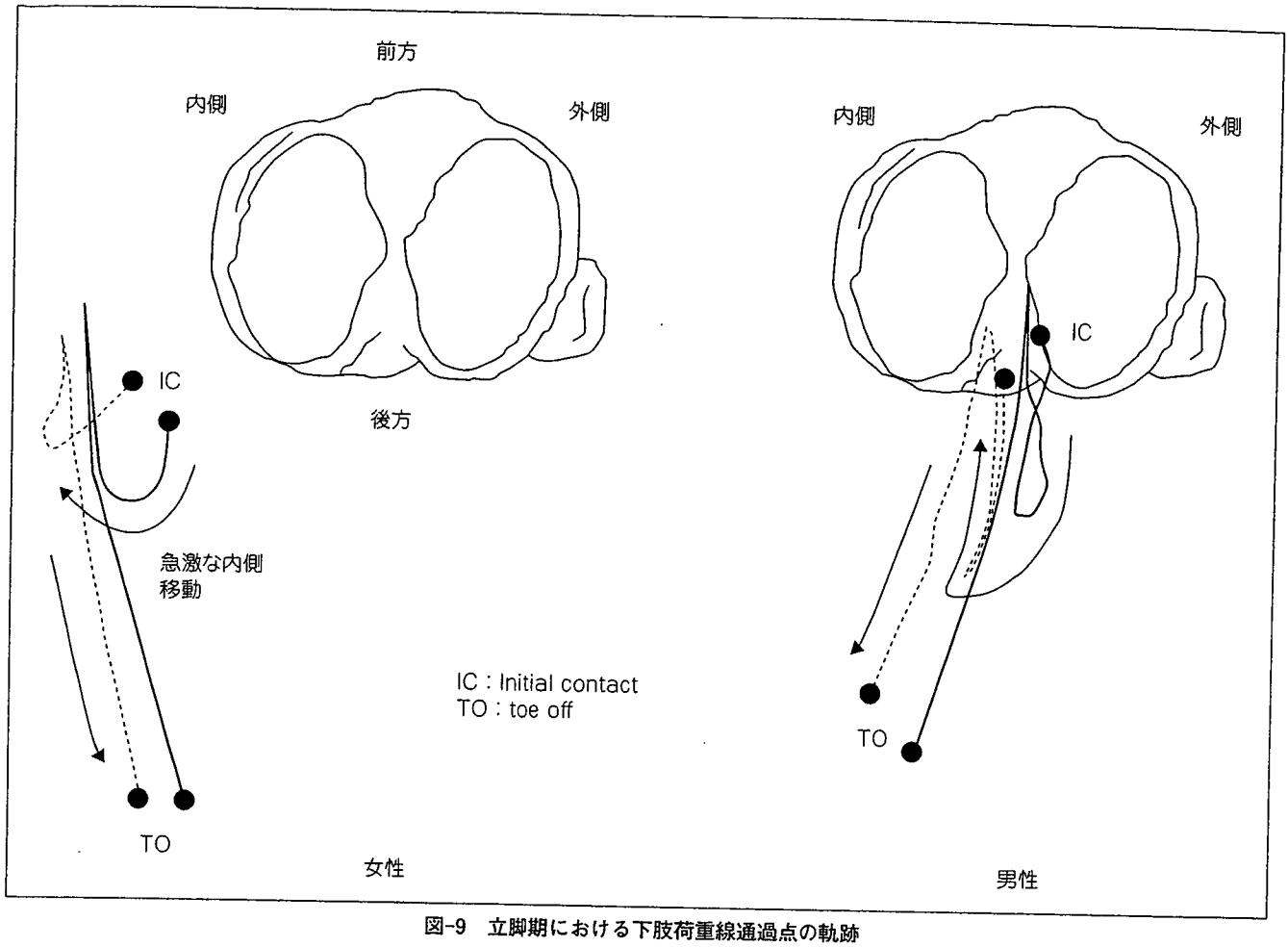

図-9　立脚期における下肢荷重線通過点の軌跡
破線が装具なし，実線が装具あり．

c．結果と考察

静的下肢アライメントでは，装具装着により全対象で大腿脛骨角の外反(女性1.1度，男性0.3度)と下肢荷重線通過点の外側移動(女性5.6%，男性8.8%)がみられた．回旋は，女性が内旋3.0度，男性が外旋2.2度で一定の方向性がないため，静的環境における回旋矯正の効果を判定し得なかった．

動的な歩行運動の結果である**図-8**は，大腿骨の内外顆軸を脛骨関節面に投影したもので，この軌跡の追跡による大腿骨回旋の解析を目的とした．装具装着によって回旋が外旋方向へわずかに増加していることが判明した．**図-9**は，立脚期における下肢荷重線通過点の軌跡を示したものである．女性の結果では脛骨内側を大きく超えて位置しており，さらに立脚初期ではスラストがみられた．装具装着によって下肢荷重線通過点が全体的に外側へ移動し，スラストもわずかに低減した．

これらの結果から，まだ検証例は少ないが異なる方法を組み合わせて運動と力学的環境変化を詳細に解析することで膝装具の効果を検討できうる可能性があると考えている．

装具研究の今後の課題

最近の膝装具は機能性だけでなく，耐久性や軽量性，デザイン性を求めたものも出始めている．その中で機能性については疼痛軽減と膝OA進行の防止を目的に膝OA患者の利益に基づいて備えるべきものであるため，その効果について運動学的・動力学的検証を詳細に行う必要がある．検証に用いる方法も膝OAの運動学的・動力学的特徴が三次元的に渡っていることから，三次元的手法が必要不可欠である．われわれは，この観

点から静的かつ動的環境下における膝装具の効果を三次元的に分析するために，いくつか方法論を開発して検討してきた．しかし，作用機序の検討で示したように，各個体にあった膝装具に必要な機能的要素を科学的に分析できてはいない．

高齢社会で多くの患者が生活する今日において，膝OAの増加に伴って装具の利用も増え，商業ベースにおいて多くの開発がなされている．しかし，膝OA患者に対して装具の効果を説明するだけの科学的な検討が少ないことは社会的な問題と考えている．装具開発ならびに装具療法を与える関係者は，さまざまな方法を駆使して長期的かつ詳細に分析し続ける姿勢が重要である．

謝　辞

膝装具の検討に協力していただいたアルケア社とSmith&Nephew社，㈱啓愛義肢材料販売所，㈱田村義肢製作所に感謝の意を示す．

文　献

1) 渡辺博史ら：変形性膝関節症の自然経過と運動療法．MB. Medical Rehabilitation 63：1-7, 2006.
2) 戸田佳孝ら：変形性膝関節症に対する装具療法研究の近年の進歩について．整形外科 57(5)：497-502, 2006.
3) Finger, S. et al.：Clinical and biomechanical evaluation of the unloading brace. The Journal of Knee Surgery 15(3)：155-159, 2002.
4) Brouwer, R. W. et al.：Brace treatment for osteoarthritis of the knee：A prospective randomized multi-centre trial. Osteoarthritis and Cartilage 14(8)：777-783, 2006.
5) Pollo, F. E. et al.：Reduction of medial compartment loads with valgus bracing of the osteoarthritic knee. The American Journal of Sports Medicine 30(3)：414-421, 2002.
6) Komistek, R. D. et al.：An in vivo analysis of the effectiveness of the osteoarthritic knee brace during heel-strike of gait. The Journal of Arthroplasty 14(6)：738-742, 1999.
7) Nadaud, M. C. et al.：In vivo three-dimensional determination of the effectiveness of the osteoarthritic knee brace：A multiple brace analysis. The Journal of Bone & Joint Surgery 87A(S2)：114-119, 2005.
8) 寺島和浩ら：変形性膝関節症に対する装具療法の生体力学的検討．日本臨床バイオメカニクス学会誌 20：459-463, 1999.
9) 大森　豪ら：変形性膝関節症用装具の効果に対する運動学的検討．日本機械学会第4回バイオエンジニアリングシンポジウム講演論文集：221-222, 1995.
10) 古賀良生ら：変形性膝関節症の運動解析．関節外科 16(3)：327-333, 1997.
11) 瀧上秀威ら：三次元動作解析装置VICONを用いた内側型変形性膝関節症患者の膝の歩行時側方動揺．日本臨床バイオメカニクス学会誌 17：213-217, 1996.
12) 木藤伸宏ら：加速度センサーを用いた変形性膝関節症の歩行時下腿運動の解析．理学療法学 31(1)：86-94, 2004.
13) 長崎浩爾ら：変形性膝関節症に対する装具療法の効果発現機序に関する生体力学的検討．日本臨床バイオメカニクス学会誌 21：247-252, 2000.

Mol. Cells, Vol. 25, No. 1, pp. 1-6

Minireview

Molecules and Cells

Endochondral Ossification Signals in Cartilage Degradation During Osteoarthritis Progression in Experimental Mouse Models

Hiroshi Kawaguchi*

Sensory and Motor System Medicine, Faculty of Medicine, University of Tokyo, Tokyo 113-8655, Japan.

(Received January 26, 2008; Accepted January 28, 2008)

Osteoarthritis (OA), one of the most common skeletal disorders characterized by cartilage degradation and osteophyte formation in joints, is induced by accumulated mechanical stress; however, little is known about the underlying molecular mechanism. Several experimental OA models in mice by producing instability in the knee joints have been developed to apply approaches from mouse genetics. Although proteinases like matrix metalloproteinases and aggrecanases have now been proven to be the principal initiators of OA progression, clinical trials of proteinase inhibitors have not been successful for the treatment, turning the interest of researchers to the upstream signals of proteinase induction. These signals include undegraded and fragmented matrix proteins like type II collagen or fibronection that affects chondrocytes through distinct receptors. Another signal is pro-inflammatory factors that are produced by chondrocytes and synovial cells; however, recent studies that used mouse OA models in knockout mice did not support that these factors have a role in the central contribution to OA development. Our mouse genetic approaches found that the induction of a transcriptional activator Runx2 in chondrocytes under mechanical stress contributes to the pathogenesis of OA through chondrocyte hypertrophy. In addition, chondrocyte apoptosis has recently been identified as being involved in OA progression. We hereby propose that these endochondral ossification signals may be important for the OA progression, suggesting that the related molecules can clinically be therapeutic targets of this disease.

Keywords: Apoptosis; Cartilage; Chondrocytes; Endochondral Ossification; Hypertrophy; Osteoarthritis.

* To whom correspondence should be addressed.
Tel: 81-33815-5411; Fax: 81-33818-4082
E-mail: kawaguchi-ort@h.u-tokyo.ac.jp

Osteoarthritis (OA) and the experimental mouse models

OA, which affects all joints of the body, is characterized by two aspects: one is cartilage degradation shown as a joint space narrowing on radiographs, and the other is osteophyte formation at the edge of the joints (Fig. 1). Despite significant social demand for more information, risk factors of this disease identified by epidemiologic studies have to date been limited to age, obesity, trauma history, occupation, and gender (Sharma et al., 2007). These factors are closely related to the accumulation of mechanical stress to joints.

In an effort to clarify the mechanisms whereby the mechanical stress leads to OA development, experimental animal models in which joint instability is induced through surgical intervention have been developed in dogs, rabbits, guinea pigs and rats (Bluteau et al., 2002; Hayami et al., 2004; Le Graverand et al., 2002; Lorenz et al., 2005; Matyas et al., 1999; 2002; Pond et al., 1973). Considering that mouse is now the most ideal animal for the molecular study due to recent progress in mouse genetics and the availability of transgenic and knockout mice, we and others have established mechanical instability-induced OA models in mice that are reproducible and resemble human OA, using a microsurgical technique to produce instability in the knee joints. Most popular is the model developed by Glasson's group which involves destabilization of the medial meniscus (DMM) by transection of meniscotibial ligament anchoring the medial meniscus to the tibial

Abbreviations: ACLT, anterior cruciate ligament transection; ADAMTS, a disintegrin and metalloproteinase thrombospondin; COL10, type X collagen; COL2, type II collagen; DDR-2, discoidin domain receptor-2; DMM, destabilization of medial meniscus; IL, interleukin; MMP, matrix metalloprotainese; OA, Osteoarthritis; PG, prostaglandin; RANKL, receptor activator of NF-kappaB ligand; TNF-α, tumor necrosis factor-α; TRAIL, tumor necrosis factor-related apoptosis-inducing ligand.

Fig. 1. Radiographs of osteoarthritis (OA) in hip, knee, lumbar spine, and hand. Cartilage degradation shown as joint space narrowing and osteophyte formation at the edge of the joints are two major disorders of OA.

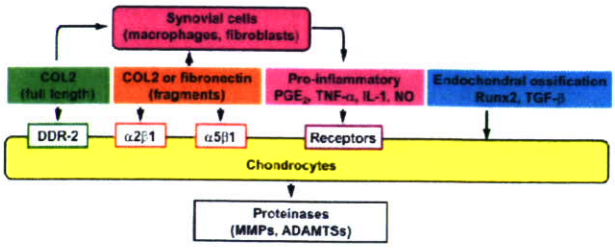

Fig. 2. Upstream signals of the induction of proteinases in chondrocytes. Matrix proteins, pro-inflammatory factors, and endochondral ossification signals are principal pathways.

plateau (Glasson et al., 2007, *ibid*). We have developed the medial model by resection of the medial meniscus and medial colateral ligament (Kamekura et al., 2005). In addition, there is a traditional anterior cruciate ligament transection (ACLT) model that has also been used in larger animals (Clements et al., 2003).

Proteinases for OA induction

Normal joint cartilage is constituted of a framework of type II collagen (COL2), in which proteoglycans connected to hyaluronic acid waves smoothly. Because proteoglycans contain a large quantity of water, they provides elasticity and lubricity to the joint surface. However, in the OA cartilage, most of the proteoglycans are cut, fragmented, and floating in the synovial fluid. Due to the loss of the shock-absorber, the mechanical stress is loaded directly onto COL2, which is also cut and degraded. It has been shown that the initiation of OA occurs with the appearance of proteinases such as matrix metalloproteinases (MMPs) and aggrecanases that sever the core proteins of proteoglycans at their specific cleavage sites (Little et al., 2007). Actually, the importance of a proteinase, ADAMTS5, also called aggrecanase-2, was proved by back-to-back publications in 2005 (Glasson et al., 2005; Stanton et al., 2005), creating a DMM model in knockout mice which showed resistance to cartilage degradation under the OA induction. However, the clinical trials of the proteinase inhibitors for the OA treatment have not been successful due to side effects like musculoskeletal pain, tendinitis, and so on (Burrage et al., 2007; Nagase et al., 2006). Hence, researchers are now turning their attention to the signals inducing the proteinases in chondrocytes; Figure 2 summarizes the upstream signals that may cause this induction. Olsen's group and others have shown that matrix protein, especially undegraded COL2, may initiate it through a receptor tyrosine kinase discoidin domain receptor 2 (DDR-2) (Li et al., 2007; Xu et al., 2005; 2007). This causes the degradation of matrix proteins, and the product fragments of COL2 or fibronection then induce proteinases through respective integrins $\alpha2\beta1$ and $\alpha5\beta1$ (Li et al., 2007).

Pro-inflammatory factors and OA

Besides these matrix proteins, pro-inflammatry factors like prostaglandins (PGs), tumor necrosis factor-α (TNF-α), interleukin-1 (IL-1), IL-6, and nitric oxides are reported to induce proteinases through their respective receptors (Vincenti et al., 2002). These pro-inflammatory factors are also reported to be produced by synovial cells under the stimulation of the undegraded or fragmented matrix proteins (Li et al., 2007). However, it is suspected that these cytokines play significant roles in the OA development. Our previous report showed that levels of TNF-α, IL-1, IL-6 as well as fibroblast growth factor-2 in the synovial fluid from knee joints of OA patients were much lower than those of rheumatoid arthritis patients (Manabe et al., 1999). Furthermore, a previous report using a mouse ACLT model showed that mice lacking IL-1, IL-1-converting enzyme, stromelysin 1 or inducible nitric oxide synthase unexpectedly exhibited an acceleration of cartilage degradation, implying that these pro-inflammatory factors do not stimulate, but rather inhibit such degradation (Clements et al., 2003).

PGE_2, a representative pro-inflammatory factor, is produced more abundantly in the OA cartilage than in normal cartilage (Jacques et al., 1999), and microsomal PGE synthase-1 (mPGES-1) is a terminal enzyme for the PGE_2 production in chondrocytes of OA patients (Kojima et al., 2004). Although we created the medial OA model in the PGES-1 knockout mice, the cartilage degradation and osteophyte formation were comparable to the wil-type littemates (Yamakawa et al., 2008) (Fig. 3). We therefore believe that inflammation may be associated with the OA process as a consequence, but might not have a central role in the cause of OA initiation or progression.

Chondrocyte hypertrophy and OA

Our examination of the time course of histology of the

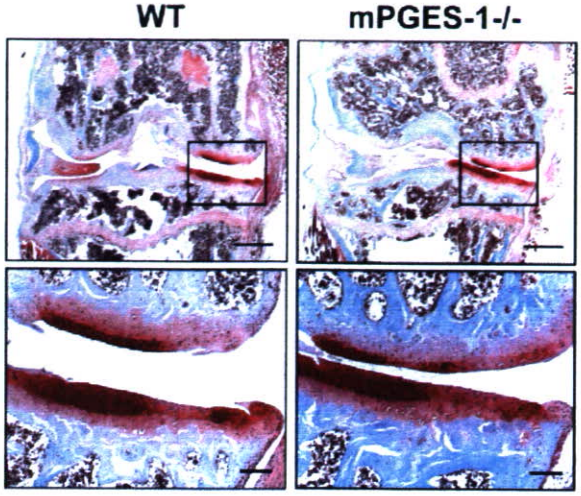

Fig. 3. Cartilage degradation in the medial portion of tibial cartilage during the OA development in the mouse medial model (Safranin O staining). Eight-week-old male WT and mPGES-/- mice underwent medial collateral ligament transaction and medial meniscus resection in the right knee joint. The inset boxes indicate the regions of the lower panels. Bars, 500 μm (upper) & 50 μm (lower).

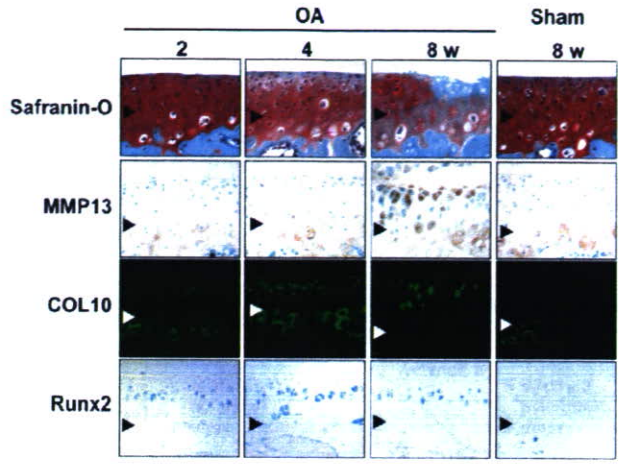

Fig. 4. Time course of expressions of MMP-13, COL10, and Runx2 in the medial tibial cartilage of OA-induced and sham-operated knee joints in the mouse medial model. Localization of MMP-13 and COL10 was detected by immunohistochemistry, and Runx2 localization was detected by X-gal staining of heterozygous Runx2 deficient mice with LacZ knock-in at the site of Runx2 deletion (Runx2+/lacz). Arrowheads indicate the level of tidemark.

mouse joint cartilage using the medial OA model revealed that type X collagen (COL10) and MMP-13 were significantly induced during OA progression (Fig. 4) (Kamekura et al., 2005; 2006). COL10 expression, a specific marker of hypertrophic chondrocytes, appeared in the superficial and middle zones above the tidemark at 4 weeks, consistent with previous studies (Boos et al., 1999; von der Mark et al., 1992). MMP-13 expression appeared in the hypertrophic chondrocytes above the tidemark at 8 weeks. These findings suggest that articular chondrocytes undergo hypertrophic differentiation in response to joint instability, and the hypertrophic chondrocytes express MMP-13 that may degrade the cartilage matrix.

Since a transcriptional activator Runx2 has been known to induce both chondrocyte hypertrophy and MMP-13 expression (Jimenez et al., 1999; Takeda et al., 2001; Ueta et al., 2001), we then examined the involvement of Runx2 during OA development (Kamekura et al., 2006). Runx2 expression was induced above the tidemark in the cartilage as early as 2 weeks, enhanced at 4 weeks, and decreased thereafter by the OA induction, which was not observed in the sham-operated cartilage (Fig. 4). For the functional analyses of Runx2, we used heterozygous Runx2-knockout mice (Runx2+/–), since homozygous Runx2-knockout (Runx2–/–) mice died just after birth. The Runx2+/– mice showed normal skeletal development and articular cartilage under physiological conditions. Both COL10 and MMP-13 expressions were decreased by the Runx2 insufficiency (data not shown), indicating that chondrocyte hypertrophy and MMP-13 induction during OA progression is at least partly mediated by Runx2. When the OA progression was compared between WT and Runx2+/– joints, the cartilage degradation in Runx2+/– was much milder than that of the WT cartilage at 8 weeks and thereafter (Fig. 5A). The Runx2+/– joint also showed decreased osteophyte formation (Fig. 5B). These findings demonstrate that Runx2 contributes to cartilage degradation and the subsequent osteophyte formation under joint instability.

Our differential display analysis identified a novel molecule that was up-regulated by a high phosphate diet in association with calcification of auricular cartilage in mice, and we called it carminerin (Koshizuka et al., 2003; Okawa et al., 1998). The knockout (carminerin –/–) mice did not show skeletal abnormality under physiological conditions. When we created the ACLT OA model, the joint destruction normally occurred; however, osteophyte formation seemed to be decreased by the knockout, indicating that carminerin is not essential for cartilage degradation but plays a role in osteophyte formation (Fig. 6) (Yamada et al., 2006).

Chondrocyte apoptosis and OA

In addition to hypertrophic differentiation of chondrocytes, chondrocyte apoptosis is known to be involved in OA development (Kühn et al., 2004). Intraarticular injection of a pan-caspase inhibitor has been reported to suppress cartilage degradation under OA induction in a rabbit

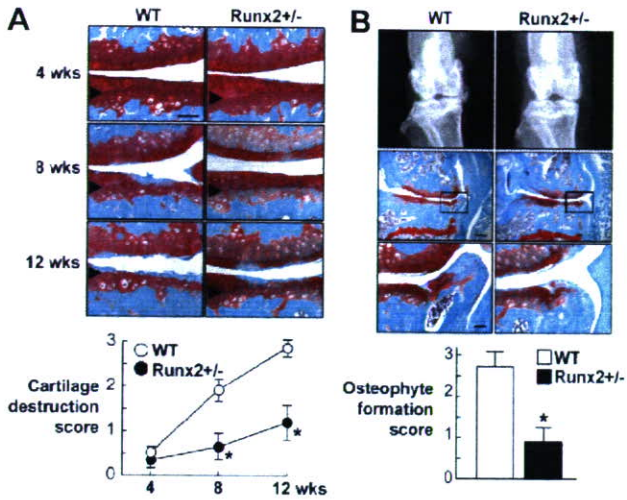

Fig. 5. A. Safranin-O staining and the cartilage degradation score of the medial tibial cartilage of Runx2–/– and wild-type (WT) littermates. Arrowheads indicate the level of tidemark. **B.** Anteroposterior X-ray features, Safranin-O staining, and the osteophyte formation score 12 weeks after surgery. Means (symbols or bars) ± SEM (error bars). * $P < 0.01$ vs. WT.

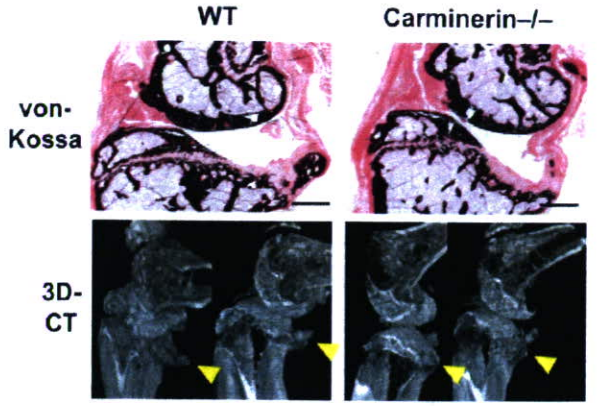

Fig. 6. von Kossa staining and three-dimensional computed tomography (3D-CT) of knee joints of carminerin–/– and wild-type (WT) littermates in the ACLT model. OA was induced at the posterior tibias of the knee joint of 8-week-old mice and examined 10 weeks after surgery.

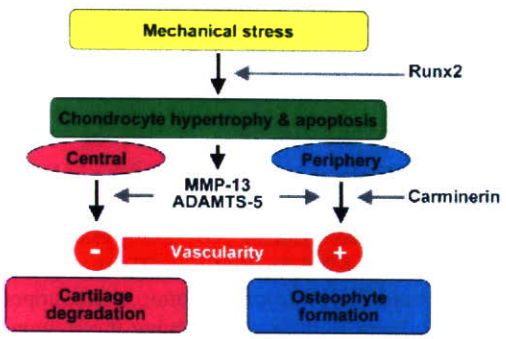

Fig. 7. Molecular background of OA progression under mechanical stress by mouse genetics approaches.

ACLT model (D'Lima et al., 2006). When we created the OA medial model in the hetero knockout mice of osteoprotegerin that is well known as a decoy receptor of RANKL for osteoclastic bone resorption, joint destruction was enhanced as compared to the wild-type littermates (Shimizu et al., 2007). On the contrary, an intraarticular injection of recombinant osteoprotegerin suppressed joint destruction with a decrease of apoptotic chondrocytes. Since tumor necrosis factor-related apoptosis-inducing ligand (TRAIL), a ligand of osteoprotegerin, induces chondrocyte apoptosis (Lee et al., 2004; Pettersen et al., 2002), osteoprotegerin might inhibit the apoptosis induced by TRAIL. These *in vivo* findings clearly demonstrate that not only chondrocyte hypertrophy, but also chondrocyte apoptosis, both of which are signals of endochondral ossification, play some roles in cartilage degradation during OA development under mechanical stress.

Conclusion

Figure 7 summarizes our hypothessis of the molecular background of OA progression under mechanical stress in joints. As the mechanism involved in this stress causing protease production, in addition to matrix proteins and pro-inflammatory signals, we hereby propose the importance of chondrocyte hypertrophy and apoptosis, which are signals for endochondral ossification. The proteinases produced by hypertrophic chondrocytes cause cartilage degradation at the center of the joint and osteophyte formation at the periphery. The difference of the two sites may depend on the vascularity. At the periphery, vascularity is accessible from synovium or tendon, which causes endochondroal ossification to occur and make osteophytes, just like at the growth plate. Carminerin may play a role in the chondrocyte calcification at this stage. However, in the center, the vascularity is not accessible from the edge, so that it ends up with cartilage degradation without being replaced by bone.

The ultimate aim of our study is to identify the molecular targets for clinical treatment of OA. Although we primarily used mouse genetics approaches, we have attempted to confirm the reproducibility of the mouse findings in humans as well through human gene polymorphism or clinical biochemical studies. Among the molecules introduced in this review, there are some whose suppression ameliorated skeletal disorders under pathological conditons but did not affect physiological conditions, indicating that the treatment targeting these molecules may lead to an ideal treatment without side effects on physiological functions. In fact, clinical trials based on the present findings are currently being practically planned.

References

Bluteau, G., Gouttenoire, J., Conrozier, T., Mathieu, P., Vignon, E., Richard, M., Herbage, D., and Mallein-Gerin, F. (2002). Differential gene expression analysis in a rabbit model of osteoarthritis induced by anterior cruciate ligament (ACL) section. Biorheology *39*, 247–258.

Boos, N., Nerlich, A.G., Wiest, I., von der Mark, K., Ganz, R., and Aebi, M. (1999). Immunohistochemical analysis of type-X-collagen expression in osteoarthritis of the hip joint. J. Orthop. Res. *17*, 495–502.

Burrage, P.S. and Brinckerhoff, C.E. (2007). Molecular targets in osteoarthritis: metalloproteinases and their inhibitors. Curr. Drug Targets *8*, 293–303.

Clements, K.M., Price, J.S., Chambers, M.G., Visco, D.M., Poole, A.R., and Mason, R.M. (2003). Gene deletion of either in-terleukin-1beta, interleukin-1beta-converting enzyme, inducible nitric oxide synthase, or stromelysin 1 accelerates the development of knee osteoarthritis in mice after surgical transection of the medial collateral ligament and partial medial meniscectomy. Arthritis Rheum. *48*, 3452–3463.

D'Lima, D., Hermida, J., Hashimoto, S., Colwell, C., and Lotz, M. (2006). Caspase inhibitors reduce severity of cartilage lesions in experimental osteoarthritis. Arthritis Rheum. *54*, 1814–1821.

Glasson, S.S., Askew, R., Sheppard, B., Carito, B., Blanchet, T., Ma, H.L., Flannery, C.R., Peluso, D., Kanki, K., Yang, Z., et al. (2005). Deletion of active ADAMTS5 prevents cartilage degradation in a murine model of osteoarthritis. Nature *434*, 644–648.

Glasson, S.S., Blanchet, T.J., and Morris, E.A. (2007). The surgical destabilization of the medial meniscus (DMM) model of osteoarthritis in the 129/SvEv mouse. Osteoarthritis Cartilage *15*, 1061–1069.

Glasson, S.S. (2007). *In vivo* osteoarthritis target validation utilizing genetically-modified mice. Curr. Drug Targets *8*, 367–376.

Hayami, T., Pickarski, M., Wesolowski, G.A., McLane, J., Bone, A., Destefano, J., Rodan, G.A., and Duong, le T. (2004). The role of subchondral bone remodeling in osteoarthritis, reduction of cartilage degeneration and prevention of osteophyte formation by alendronate in the rat anterior cruciate ligament transection model. Arthritis Rheum. *50*, 1193–1206.

Jacques, C., Sautet, A., Moldovan, M., Thomas, B., Humbert, L., and Berenbaum, F. (1999). Cyclooxygenase activity in chondrocytes from osteoarthritic and healthy cartilage. Rev. Rhum. Engl. Ed. *66*, 701–704.

Jimenez, M.J., Balbin, M., Lopez, J.M., Alvarez, J., Komori, T., and Lopez-Otin, C. (1999). Collagenase 3 is a target of Cbfa1, a transcription factor of the runt gene family involved in bone formation. Mol. Cell. Biol. *19*, 4431–4442.

Kamekura, S., Hoshi, K., Shimoaka, T., Chung, U., Chikuda, H., Yamada, T., Uchida, M., Ogata, N., Seichi, A., Nakamura, K., et al. (2005). Osteoarthritis development in novel experimental mouse models induced by knee joint instability. Osteoarthritis Cartilage *13*, 632–641.

Kamekura, S., Kawasaki, Y., Hoshi, K., Shimoaka, T., Chikuda, H., Maruyama, Z., Komori, T., Sato, S., Takeda, S., Karsenty, G., et al. (2006). Runx2 contributes to pathogenesis of osteoarthritis in mice after induction of knee joint instability. Arthritis Rheum. *54*, 2462–2470.

Kojima, F., Naraba, H., Miyamoto, S., Beppu, M., Aoki, H., and Kawai, S. (2004). Membrane-associated prostaglandin E synthase-1 is upregulated by proinflammatory cytokines in chondrocytes from patients with osteoarthritis. Arthritis Res. Ther. *6*, R355–365.

Koshizuka, Y., Yamada, T., Hoshi, K., Ogasawara, T., Chung, U., Kawano, H., Nakamura, Y., Nakamura, K., Ikegawa, S., and Kawaguchi, H. (2003). Cystatin 10, a novel chondrocyte-specific protein, may promote the last steps of the chondrocyte differentiation pathway. J. Biol. Chem. *278*, 48259–48266.

Kühn, K., D'Lima, D.D., Hashimoto, S., and Lotz, M. (2004). Cell death in cartilage. Osteoarthritis Cartilage *12*, 1–16.

Le Graverand, M.P., Eggerer, J., Vignon, E., Otterness, I.G., Barclay, L., and Hart, D.A. (2002). Assessment of specific mRNA levels in cartilage regions in a lapine model of osteoarthritis. J. Orthop. Res. *20*, 535–544.

Lee, S.W., Lee, H.J., Chung, W.T., Choi, S.M., Rhyu, S.H., Kim, D.K., Kim, K.T., Kim, J.Y., Kim, J.M., and Yoo, Y.H. (2004). TRAIL induces apoptosis of chondrocytes and influences the pathogenesis of experimentally induced rat osteoarthritis. Arthritis Rheum. *50*, 534–542.

Li, Y., Xu, L., and Olsen, B.R. (2007). Lessons from genetic forms of osteoarthritis for the pathogenesis of the disease. Osteoarthritis Cartilage *15*, 1101–1105.

Little, C.B., Meeker, C.T., Golub, S.B., Lawlor, K.E., Farmer, P.J., Smith, S.M., and Fosang, A.J. (2007). Blocking aggrecanase cleavage in the aggrecan interglobular domain abrogates cartilage erosion and promotes cartilage repair. J. Clin. Invest. *117*, 1627–1636.

Lorenz, H., Wenz, W., Ivancic, M., Steck, E., and Richter, W. (2005). Early and stable upregulation of collagen type II, collagen type I and YKL40 expression levels in cartilage during early experimental osteoarthritis occurs independent of joint location and histological grading. Arthritis Res. Ther. *7*, R156–165.

Manabe, N., Oda, H., Nakamura, K., Kuga, Y., Uchida, S., and Kawaguchi, H. (1999). Involvement of fibroblast growth factor-2 in joint destruction of rheumatoid arthritis patients. Rheumatology (Oxford). *38*, 714–720.

Matyas, J.R., Ehlers, P.F., Huang, D., and Adams, M.E. (1999). The early molecular natural history of experimental osteoarthritis. I. Progressive discoordinate expression of aggrecan and type II procollagen messenger RNA in the articular cartilage of adult animals. Arthritis Rheum. *42*, 993–1002.

Matyas, J.R., Huang, D., Chung, M., and Adams, M.E. (2002). Regional quantification of cartilage type II collagen and aggrecan messenger RNA in joints with early experimental osteoarthritis. Arthritis Rheum. *46*, 1536–1543.

Nagase, H., Visse, R., and Murphy, G. (2006). Structure and function of matrix metalloproteinases and TIMPs. Cardiovasc. Res. *69*, 562-573.

Okawa. A., Nakamura, I., Goto, S., Moriya, H., Nakamura, Y., and Ikegawa, S. (1998). Mutation in Npps in a mouse model of ossification of the posterior longitudinal ligament of the spine. Nat. Genet. *19*, 271–273.

Pettersen, I., Figenschau, Y., Olsen, E., Bakkelund, W., Smedsröd, B., and Sveinbjörnsson, B. (2002). Tumor necrosis factor-related apoptosis-inducing ligand induces apoptosis in human articular chondrocytes *in vitro*. Biochem. Biophys.

Res. Commun. *296*, 671–676.

Pond, M.J. and Nuki, G. (1973). Experimentally-induced osteoarthritis in the dog. Ann. Rheum. Dis. *32*, 387–388.

Sharma, L. and Kapoor, D. (2007). Epidemiology of osteoarthritis. In, Moskowitz R.W. Altman R.D. Hochberg M.C. Buckwalter J.A. Goldberg V.M. editors. In Osteoarthritis, Diagnosis and Medical/ Surgical Management. 4th ed., R.W. Moskowitz, R.D. Altman, M.C. Hochberg, J.A. Buckwalter, and V.M. Goldberg, eds. (Philadelphia, USA: Lippincott Williams & Wilkins), pp. 3–26.

Shimizu, S., Asou, Y., Itoh, S., Chung, U.I., Kawaguchi, H., Shinomiya, K., and Muneta, T. (2007). Prevention of cartilage degradation with intraarticular osteoclastogenesis inhibitory factor/osteoprotegerin in a murine model of osteoarthritis. Arthritis Rheum. *56,* 3358–3365.

Stanton, H., Rogerson, F.M., East, C.J., Golub, S.B., Lawlor, K.E., Meeker, C.T., Little, C.B., Last, K., Farmer, P.J., Campbell, I.K., et al. (2005). ADAMTS5 is the major aggrecanase in mouse cartilage *in vivo* and *in vitro*. Nature *434*, 648–652.

Takeda, S., Bonnamy, J.P., Owen, M.J., Ducy, P., and Karsenty, G. (2001). Continuous expression of Cbfa1 in nonhypertrophic chondrocytes uncovers its ability to induce hypertrophic chondrocyte differentiation and partially rescues Cbfa1-deficient mice. Genes Dev. *15*, 467–481.

Ueta, C., Iwamoto, M., Kanatani, N., Yoshida, C., Liu, Y., Enomoto-Iwamoto, M., Ohmori, T, Enomoto, H., Nakata, K., Takada, K., et al. (2001). Skeletal malformations caused by overexpression of Cbfa1 or its dominant negative form in chondrocytes. J. Cell Biol. *153*, 87–100.

Vincenti, M.P. and Brinckerhoff, C.E. (2002). Transcriptional regulation of collagenase (MMP-1. MMP-13) genes in arthritis, integration of complex signaling pathways for the recruitment of gene-specific transcription factors. Arthritis Res. *4*, 157–164.

von der Mark, K., Kirsch, T., Nerlich, A., Kuss, A., Weseloh, G., Gluckert, K., and Stöss, H. (1992). Type X collagen synthesis in human osteoarthritic cartilage. Indication of chondrocyte hypertrophy. Arthritis Rheum. *35*, 806–811.

Xu, L., Peng, H., Wu, D., Hu, K., Goldring, M.B., Olsen, B.R., and Li, Y. (2005). Activation of the discoidin domain receptor 2 induces expression of matrix metalloproteinase 13 associated with osteoarthritis in mice. J. Biol. Chem. *280*, 548–555.

Xu, L., Peng, H., Glasson, S., Lee, P.L., Hu, K., Ijiri, K., Olsen, B.R., Goldring, M.B., and Li, Y. (2007). Increased expression of the collagen receptor discoidin domain receptor 2 in articular cartilage as a key event in the pathogenesis of osteoarthritis. Arthritis Rheum. *56*, 2663–2673.

Yamada, T., Kawano, H., Koshizuka, Y., Fukuda, T., Yoshimura, K., Kamekura, S., Saito, T., Ikeda, T., Kawasaki, Y., Azuma, Y., et al. (2006). Carminerin contributes to chondrocyte calcification during endochondral ossification. Nat. Med. *12*, 665–670.

Yamakawa, K., Kamekura, S., Kawamura, N., Saegusa, M., Kamei, D., Murakami, M., Kudo, I., Uematsu, S., Akira, S., Chung, U.I., et al. (2008). Association of microsomal prostaglandin E synthase 1 deficiency with impaired fracture healing, but not with bone loss or osteoarthritis, in mouse models of skeletal disorders. Arthritis Rheum. *58*, 172–183.

ARTHRITIS & RHEUMATISM
Vol. 58, No. 1, January 2008, pp 172–183
DOI 10.1002/art.23158

Association of Microsomal Prostaglandin E Synthase 1 Deficiency With Impaired Fracture Healing, But Not With Bone Loss or Osteoarthritis, in Mouse Models of Skeletal Disorders

Kiyofumi Yamakawa,[1] Satoru Kamekura,[1] Naohiro Kawamura,[1] Masatomo Saegusa,[1] Daisuke Kamei,[2] Makoto Murakami,[3] Ichiro Kudo,[2] Satoshi Uematsu,[4] Shizuo Akira,[4] Ung-il Chung,[1] Kozo Nakamura,[1] and Hiroshi Kawaguchi[1]

Objective. **Prostaglandin E synthase (PGES) functions as the terminal enzyme in the biosynthesis of prostaglandin E_2 (PGE_2) and is a potent regulator of bone and cartilage metabolism. Among the 3 isozymes of PGES, microsomal PGES-1 (mPGES-1) is known to play the most critical role in the production of PGE_2 in pathophysiologic events. This study investigated the roles of mPGES-1 under normal physiologic and pathophysiologic conditions in the skeletons of mPGES-1–deficient (mPGES-$1^{-/-}$) mice.**

Methods. **Skeletons of mPGES-$1^{-/-}$ mice and their wild-type littermates were compared by radiologic and histologic analyses. Four models of skeletal disorders were created: bone loss induced by ovariectomy, bone loss induced by hind limb unloading, osteoarthritis (OA) induced by instability in the knee joint, and bone fracture by osteotomy at the tibial midshaft. Expression of the PGES enzymes was examined by immunohistochemistry and real-time reverse transcription–polymerase chain reaction. The cellular mechanism of fracture healing was examined in ex vivo cultures of costal cartilage chondrocytes.**

Results. **Microsomal PGES-$1^{-/-}$ mice had unaffected skeletal phenotypes under normal physiologic conditions. In the bone fracture model, fracture healing was impaired by the mPGES-1 deficiency, with half of the mice remaining in a non–bone union state even after 21 days; normal fracture healing was restored by adenoviral reintroduction of mPGES-1. The other skeletal disorders were not affected by the mPGES-1 deficiency. In vivo and ex vivo analyses revealed an impaired proliferation of chondrocytes in cartilage with the mPGES-1 deficiency, at an early stage of fracture healing.**

Conclusion. **In these mouse models of skeletal disorders, mPGES-1 was indispensable for bone repair through chondrocyte proliferation, but was not essential for the skeleton under normal physiologic conditions, nor did it play a role in the pathophysiologic conditions of bone loss due to ovariectomy, bone loss due to unloading, or stress-induced OA.**

Prostaglandin E_2 (PGE_2) is produced in many types of tissue, including bone and cartilage, and has a broad range of biologic activities that are carried out via binding to 4 different G protein–coupled receptors, EP1, EP2, EP3, and EP4, which are linked to different intracellular signaling pathways (1,2). In the biosynthesis of PGE_2, 3 enzymatic steps have been identified, involving phospholipase A_2, cyclooxygenase (COX), and prostaglandin E synthase (PGES).

PGES, the terminal enzyme that catalyzes the conversion of PGH_2 to PGE_2, exists as 2 membrane-associated enzymes, microsomal PGES-1 (mPGES-1)

Supported by a Grant-in-Aid for Scientific Research from the Japanese Ministry of Education, Culture, Sports, Science, and Technology (14370452).

[1]Kiyofumi Yamakawa, MD, PhD, Satoru Kamekura, MD, PhD, Naohiro Kawamura, MD, Masatomo Saegusa, MD, PhD, Ung-il Chung, MD, PhD, Kozo Nakamura, MD, PhD, Hiroshi Kawaguchi, MD, PhD: University of Tokyo, Tokyo, Japan; [2]Daisuke Kamei, PhD, Ichiro Kudo, PhD: Showa University, Tokyo, Japan; [3]Makoto Murakami, PhD: Tokyo Metropolitan Institute of Medical Science, Tokyo, Japan; [4]Satoshi Uematsu, MD, PhD, Shizuo Akira, MD, PhD: Osaka University, Osaka, Japan.

Address correspondence and reprint requests to Hiroshi Kawaguchi, MD, PhD, Sensory and Motor System Medicine, Faculty of Medicine, University of Tokyo, Hongo 7-3-1, Bunkyo, Tokyo 113-8655, Japan. E-mail: kawaguchi-ort@h.u-tokyo.ac.jp.

Submitted for publication March 5, 2007; accepted in revised form September 21, 2007.

and mPGES-2, and 1 cytosolic enzyme, cPGES (3–9). Microsomal PGES-1 is a glutathione (GSH)–requiring perinuclear protein that belongs to the family of MAPEGs (membrane-associated proteins involved in eicosanoid and GSH metabolism), is induced by proinflammatory stimuli and suppressed by glucocorticoids, and is functionally coupled with COX-2 in marked preference to COX-1 (4,5). Induction of mPGES-1 expression is observed in various conditions in which COX-2–derived PGE_2 plays a critical role, such as inflammation, tissue repair, fever, pain, dysfunctioning of the female reproductive system, cancer, and bone resorption (3,10). In contrast, mPGES-2, which has a catalytic glutaredoxin- or thioredoxin-like domain, is constitutively expressed in various tissues and functionally coupled with both COX-1 and COX-2 (8,9). Cytosolic PGES, also constitutively expressed in a wide variety of cells, is functionally linked to COX-1, but not to COX-2, to promote immediate PGE_2 production (11,12).

Among the PGES enzymes, biochemical and biologic analyses have led to the proposal that mPGES-1 plays the most critical role in the production of PGE_2 in various pathophysiologic events. An initial study with mPGES-1–knockout (mPGES-$1^{-/-}$) mice revealed the essential role of mPGES-1 in lipopolysaccharide (LPS)–stimulated PGE_2 production by macrophages, although the mice remained fertile and developed and grew normally (13). Further analyses of mPGES-$1^{-/-}$ mice, performed by us and by other investigators, have shown an important role of mPGES-1 in pain sensitivity, febrile responses, and tissue granulation accompanying angiogenesis (14,15).

In bone, PGE_2 is the most abundant prostanoid and strongly regulates both bone resorption and bone formation (1). We previously reported that mPGES-1 is induced by bone-resorptive cytokines, preceded by the induction of COX-2, in osteoblasts, and that the induction of mPGES-1 mediates the catabolic effects of the osteoblasts (10). Similar to mice deficient in COX-2 and EP4 (2,16), mPGES-$1^{-/-}$ mice were shown to be resistant to LPS-induced bone resorption (17).

PGE_2 is also known to be a potent stimulator of bone formation (1), so that selective agonists of EP2 and EP4 stimulate bone formation (2,18). Although recent studies of PGE_2 receptor–knockout or COX-2–knockout mice failed to demonstrate abnormalities in skeletal development or growth, bone formation was impaired by the deficiency under pathologic conditions (2,19,20).

PGE_2 is also known to have a role in both catabolic and anabolic regulation of chondrocyte functions (21). In joint cartilage, it acts as one of the major catabolic mediators involved in cartilage degradation (22–24). Studies of knockout mice revealed the contributory roles of mPGES-1 and EP4 to collagen-induced arthritis (CIA) (14,15,25). In addition, PGE_2 is produced more abundantly in osteoarthritic (OA) cartilage than in normal cartilage (26), and mPGES-1 is a key enzyme in the regulation of PGE_2 production in chondrocytes from patients with OA (27). Thus, the present study investigated the contribution of mPGES-1 to bone and cartilage metabolism under normal physiologic and pathophysiologic conditions, by creating models of ovariectomy- or hind limb unloading–induced bone loss, joint instability–induced OA, and bone fracture in mPGES-$1^{-/-}$ mice.

MATERIALS AND METHODS

Animals. The generation of mPGES-1 gene–targeted mice has been described previously (13). In each experiment, mPGES-$1^{-/-}$ mice and their wild-type (WT) littermates were fed a standard diet. All experiments were performed according to the protocol approved by the Animal Care and Use Committee of the University of Tokyo.

Bone morphology. A bone radiograph of the whole bodies, femurs, and tibias was obtained with a soft x-ray apparatus (CMB-2; Softex, Tokyo, Japan). The bone mineral density (BMD; mg/cm^2) of the right femurs, tibias, and L2–L5 vertebral bodies was determined using dual x-ray absorptiometry (DXA) (PIXImus; Lunar, Madison, WI), according to the manufacturer's instructions. Histologic analyses were carried out on the left tibias of 8-week-old mice. For assessment of dynamic histomorphometric indices, mice were injected subcutaneously with 16 mg/kg body weight of calcein, at 10 days and 3 days before termination. Thereafter, the tibias were excised and fixed with ethanol, and the undecalcified bones were embedded in methyl methacrylate.

Six-micrometer frontal sections from the proximal parts of the tibias were stained with Villanueva-Goldner, and were visualized under light fluorescence microscopy for calcein labeling. Growth plates were stained with toluidine blue. Tartrate-resistant acid phosphatase–positive cells were stained at pH 5.0 in the presence of L(+)-tartaric acid, using naphthol-AS-MX phosphate in *N*,*N*-dimethylformamide as the substrate. The specimens were subjected to histomorphometric analyses using a semiautomated system (Osteoplan II; Carl Zeiss Instruments, Thornwood, NY). Parameters for the trabecular bone were measured in an area 1.2 mm in length to a depth 0.3 mm below the growth plate at the proximal metaphysis of the tibias.

Ovariectomy experiment. Twenty-six-week-old female mPGES-$1^{-/-}$ and WT mice underwent a bilateral ovariectomy or a sham operation under general anesthesia, as we have previously reported (28). Mice were killed 4 weeks after the surgery, and the weight of the excised uterus was measured. The BMD of the tibias was measured by DXA immediately

before the surgery and 4 weeks after surgery. Results for each mouse were calculated as the percent loss of BMD during that period.

Tail suspension experiment. Eight-week-old female mPGES-1$^{-/-}$ and WT mice were subjected to tail suspension for 4 weeks. A tape was applied to the surface of the tail for placement of a metal clip. The end of the clip was fixed to an overhead bar and the position of the tape was adjusted to maintain the mice in a 30° head-down tilt with the hind limbs elevated above the floor of the cage. For the control group, mice were housed individually under the same conditions but were not subjected to tail suspension, so that the hind limbs remained in a weight-bearing position (loaded control). After 4 weeks, the mice were killed and the right tibias were subjected to BMD measurement and histomorphometric analysis.

OA experiment. The surgical procedure to create an OA experimental model was performed on 8-week-old male mice, as we have reported previously (29–31). Briefly, mice were placed under general anesthesia and the medial collateral ligament was transected. The medial meniscus was then removed using a surgical microscope. Fourteen weeks after surgery, the mice were killed and the entire knee joints were dissected, decalcified, and stained with Safranin O–fast green. Destruction of cartilage was quantified as the most severe changes among 20 serial sections according to our original histologic grading scale of 0–4 (29), which was assessed by a single observer (SK) who was blinded to the experimental group.

Fracture experiment. A transverse osteotomy at the midshaft of the right tibia was created at the midshaft using a bone saw, and was internally stabilized with an intramedullary nail using the inner pin of a spinal needle of 22- or 23-gauge diameter, depending on the size of the cavity, as we have reported previously (30,32). The left tibia (unfractured side) was subjected to sham operation and an intramedullary nail of the same size was inserted. To determine whether there was bone union, bony bridging on radiographs was evaluated by a single observer (SK) who was blinded to the experimental group. The area and bone mineral content (BMC) of the entire tibia were measured bilaterally using DXA. The area and BMC of the tibias were measured bilaterally before and at various time points after the fracture operation, and differences in the increased values (gain of area and percent gain of BMC) between the right (fractured) tibia and left (unfractured) tibia were calculated.

For histologic analyses, specimens of the harvested tibias were fixed with 4% paraformaldehyde, decalcified with EDTA, dehydrated with ethanol, embedded in paraffin, and cut into 4-μm sections. The sections were stained with hematoxylin and eosin or toluidine blue. For immunohistochemistry, samples were examined in dewaxed paraffin–embedded sections. After dehydration, the sections were treated with 0.3% hydrogen peroxide and then with 1% bovine serum albumin, and incubated with a polyclonal rabbit antibody to mPGES-1 (Cayman Chemical, Ann Arbor, MI) or type X collagen (COL10; Santa Cruz Biotechnology, Santa Cruz, CA) at a dilution of 1:100. The sections were then incubated with horseradish peroxidase–conjugated goat antibody against rabbit IgG (Dakopatts, Glostrup, Denmark).

For bromodeoxyuridine (BrdU) labeling, mice were injected intraperitoneally with BrdU (25 μg/gram body weight) 2 hours prior to termination. Incorporated BrdU was detected using a BrdU staining kit (Zymed, San Francisco, CA). TUNEL staining was performed using an Apoptosis in Situ Detection kit (Wako Pure Chemical, Osaka, Japan) according to the manufacturer's instructions.

For measurement of PG levels, fracture callus and sham-operated sites of the tibias were homogenized 7 days after surgery in a homogenization buffer containing 10 μM indomethacin. Aliquots were then adjusted to pH 3.0 with 1N HCl and passed through Sep-Pak C18 cartridges (Cayman Chemical), and the retained PGs were eluted from the cartridges with methanol. A trace amount of ^{3}H-PGE$_2$ (Cayman Chemical) was added to the samples before passage through the cartridges, to calibrate the recovery of PGs. The solvent of the samples was evaporated, and the PGs were dissolved in an aliquot of buffer and assayed with PGE$_2$ and PGF$_{2\alpha}$ enzyme immunoassay kits (Cayman Chemical) according to the manufacturer's instructions.

Real-time reverse transcription–polymerase chain reaction (RT-PCR) analysis. Total RNA was extracted from the fracture callus by isogen–chloroform extraction and isopropanol precipitation (Nippon Gene, Tokyo, Japan), according to the manufacturer's instructions. Total messenger RNA (mRNA) (1 μg) was reverse transcribed using Superscript reverse transcriptase with random hexamer (Takara Shuzo, Shiga, Japan), and 1 μl of each reverse transcriptase reaction was used as a template for the second-step SYBR Green real-time RT-PCR. The full-length or partial-length complementary DNA of target genes, including PCR amplicon sequences, was amplified by PCR, cloned into pCR4-TOPO vectors (Invitrogen, Carlsbad, CA), and used as standard templates after linearization. QuantiTect SYBR Green PCR Master Mix (Qiagen, Chatsworth, CA) was used for the second-step SYBR Green real-time RT-PCR, according to the manufacturer's instructions. SYBR Green PCR amplification and real-time fluorescence detection were performed using an ABI Prism 7700 sequence detection system (Applied Biosystems, Foster City, CA). All reactions were run in quadruplicate.

Copy numbers of target gene mRNA in each total RNA were calculated by reference to standard curves and were adjusted to the mouse standard total RNA (Applied Biosystems) with the mouse actin as an internal control. PCR amplification was performed using the following specific primer pairs: for mPGES-1, sense 5′-TTACAGGAGTGACCCAGATGT-3′ and antisense 5′-GAGAACTGGGCCAGGACATA-3′; for mPGES-2, sense 5′-ACATCCAGCCTTGGTACCTG-3′ and antisense 5′-TGTAAGTTTGGGCCTTGTCC-3′; for cPGES, sense 5′-CGATCCAAATGATTCCAAGC-3′ and antisense 5′-CATCCTCCCAGTCTTTCCAA-3′; and for actin, sense 5′-AGATGTGGATCAGCAAGCAG-3′ and antisense 5′-GCGCAAGTTAGGTTTTGTCA-3′.

Isolation and culture of mouse costal chondrocytes. Newborn mice were killed and the costal cartilage, not including the soft tissue, was digested with 0.3% collagenase in Dulbecco's modified Eagle's medium (DMEM) (Sigma, St. Louis, MO) at 37°C for 5 hours. For the cell proliferation assay, primary chondrocytes from mPGES-1$^{-/-}$ and WT mice were incubated at a density of 5,000 cells/well in DMEM with

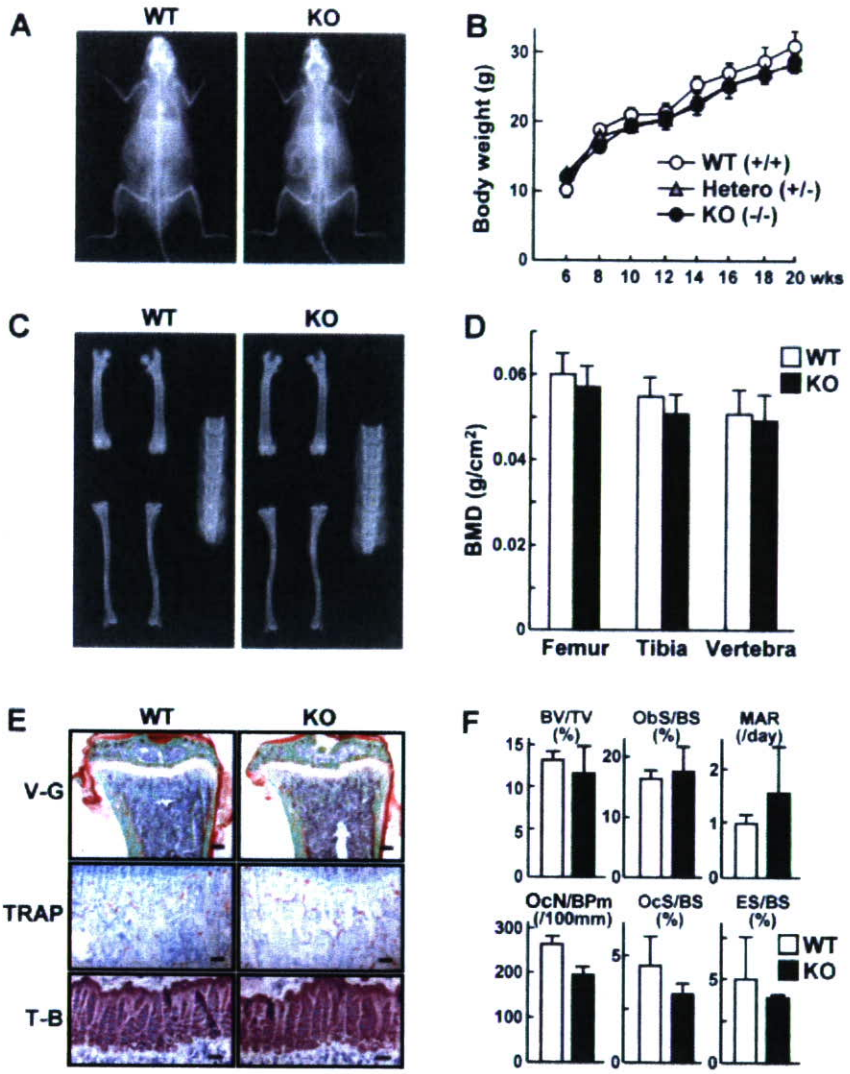

Figure 1. Radiologic and histologic findings in the bones of microsomal prostaglandin E synthase 1–knockout (KO) (mPGES-$1^{-/-}$) mice and their wild-type (WT) littermates under normal physiologic conditions. **A,** Radiologic images of the whole body of representative 8-week-old male WT and KO mice. **B,** Growth curves, as determined by body weight, of the male WT, mPGES-$1^{+/-}$, and mPGES-$1^{-/-}$ mice. Results are the mean ± SEM of 20 mice/group. **C,** Radiologic images of the femurs, tibias, and lumbar vertebrae of representative 8-week-old male WT and KO mice. **D,** Bone mineral density (BMD) of the entire femurs, tibias, and L2–L5 vertebrae, as determined by dual x-ray absorptiometry. Bars show the mean and SEM of 8 bones/group. **E,** Histologic features of the proximal tibias of WT and KO mice. With Villanueva-Goldner (V-G) staining, mineralized bone is stained green and unmineralized osteoid is stained red (bar = 200 μm). With tartrate-resistant acid phosphatase (TRAP) staining of the primary spongiosa below the growth plate, osteoclasts are stained red (bar = 50 μm). With toluidine blue (T-B) staining of the growth plate, cartilage matrix is stained purple (bar = 20 μm). **F,** Histomorphometric parameters in the proximal tibias of WT and KO mice. Bars show the mean and SEM of 3 mice/group. BV/TV = bone volume per total volume; ObS/BS = osteoblast surface per bone surface; MAR = mineral apposition rate; OcN/BPm = number of osteoclasts per 100 mm of bone perimeter; OcS/BS = osteoclast surface per bone surface; ES/BS = eroded surface per bone surface.

10% fetal bovine serum. The number of cells/well was counted using a WST-8 assay with a Cell Counting Kit 8 (Dojindo, Kumamoto, Japan), with results expressed as the absorbance of each well at 450 nm. For alkaline phosphatase staining, performed on day 14 after confluency, cultured cells were fixed in 70% ethanol and stained for 10 minutes with a solution containing 0.01% naphthol-AS-MX phosphate disodium salt (Sigma), 1% *N,N*-dimethylformamide (Wako Pure Chemical), and 0.06% Fast Blue BB. For alizarin red S staining, performed on day 21 after confluency, cells were fixed in 10% buffered

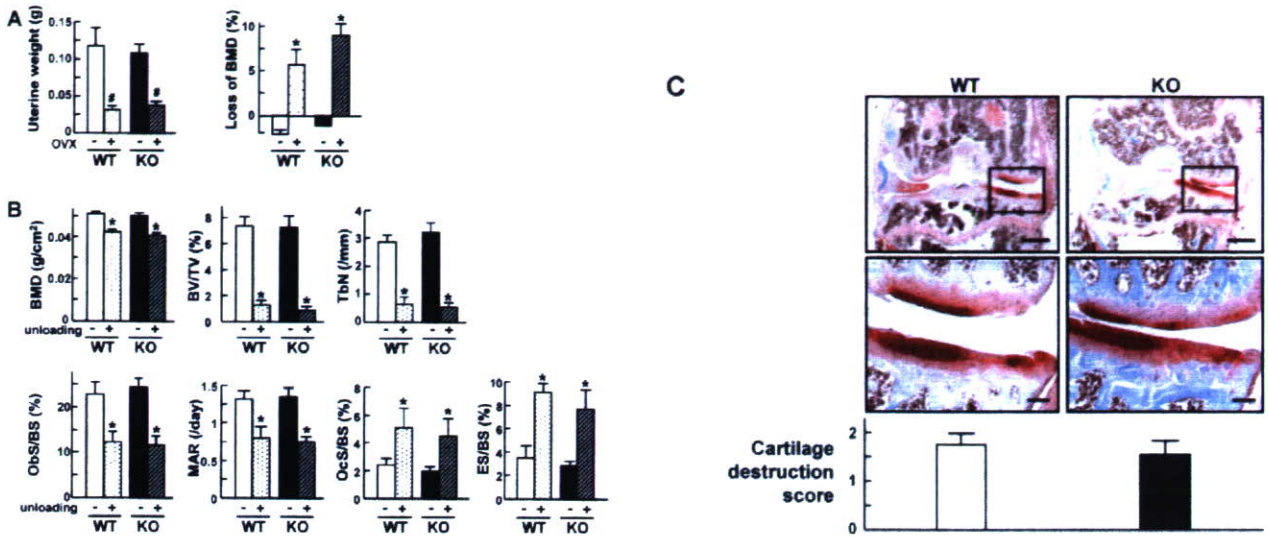

Figure 2. **A,** Effects of ovariectomy (OVX) on the bones of KO (mPGES-1$^{-/-}$) mice and their WT littermates. Female mice underwent ovariectomy (+) or sham operation (−) at age 26 weeks, and were killed at 30 weeks. Values for uterus weight at 30 weeks (left) and percentage loss of BMD of the tibia at 4 weeks after surgery (right) are the mean and SEM of 5 mice/group. There were no significant differences between the WT and mPGES-1$^{-/-}$ mice. # = $P < 0.05$; * = $P < 0.01$, versus sham-operated mice. **B,** Effects of unloading of the proximal tibias (+) of WT and mPGES-1$^{-/-}$ mice. Unloading was performed using the tail suspension model in 8-week-old female littermates, and BMD and histomorphometric parameters were assessed at 4 weeks after unloading. BMD results are the mean and SEM of 8 mice/group, while histomorphometric parameters (BV/TV, trabecular number [TbN], ObS/BS, MAR, OcS/BS, and ES/BS) are the mean and SEM of 3 mice/group. There were no significant differences between the WT and mPGES-1$^{-/-}$ mice. * = $P < 0.01$ versus loaded (−) controls. **C,** Cartilage destruction in the medial portion of the tibial cartilage during the development of osteoarthritis induced by knee joint instability. Eight-week-old male WT and mPGES$^{-/-}$ mice underwent medial collateral ligament transection and medial meniscus resection of the right knee joint. Shown are representative results from Safranin O staining of the frontal sections of the knee (top and middle) and histologic scoring of cartilage destruction (mean and SEM of 3 mice/group) (bottom) at 14 weeks after surgery. Boxed areas in the top panels are shown in higher magnification in the middle panels (top, bar = 500 μm; middle, bar = 50 μm). See Figure 1 for other definitions.

formalin and stained for 10 minutes with 2% alizarin red S (pH 4.0).

Generation of adenoviruses and gene transfer. The recombinant adenovirus vectors carrying the mPGES-1 gene (Ax-mPGES-1) and the control β-galactosidase gene (Ax-LacZ) that was engineered to express the hemagglutinin tag at its N-terminus were constructed using the Adenoviral Expression System (Invitrogen), following the manufacturer's protocol. Two days after the operation, a suspension of 10^{12} plaque-forming units of Ax-mPGES-1 or Ax-LacZ was injected into the fracture site, as described previously (33). Animals were killed 14 days after the injection, with subsequent analyses carried out as described above.

Statistical analysis. The mean values of each group were compared by analysis of variance. Significant differences between groups were determined by post hoc testing with Bonferroni's method.

RESULTS

Skeletal phenotypes of mPGES-1$^{-/-}$ mice under normal physiologic conditions. We initially analyzed the skeletons of mPGES-1$^{-/-}$ mice under normal physiologic conditions. Radiologic analyses showed no significant differences in the skeleton between mPGES-1$^{-/-}$ mice and their WT littermates (Figure 1A). The mPGES-1$^{-/-}$ mice grew normally and had no abnormalities in the major organs. Moreover, growth curves, as determined by body weight, were similar among the WT, mPGES-1$^{+/-}$, and mPGES-1$^{-/-}$ mice during an observation period of up to 20 weeks of age (Figure 1B).

The BMDs of the femurs, tibias, and lumbar vertebrae were also comparable between mPGES-1$^{-/-}$ mice and their WT littermates (Figures 1C and D). Furthermore, histologic analyses revealed no differences between groups in the bone volume or osteoclast number (Figure 1E), and these findings were supported by histomorphometric measurements that showed comparable values for bone volume (assessed as bone volume per total volume), bone formation parameters (osteoblast surface per bone surface, and mineral apposition rate), and bone resorption parameters (number of osteoclasts per 100 mm of bone perimeter, osteoclast surface

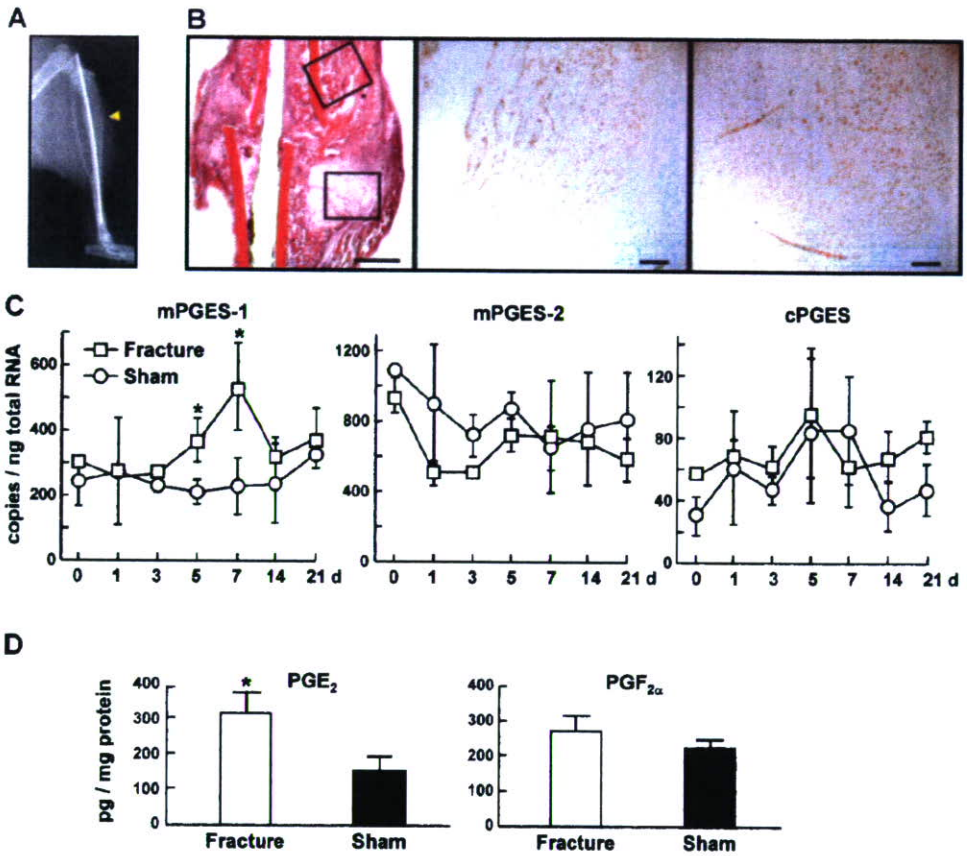

Figure 3. Expression of PGES enzymes and levels of prostaglandin E_2 (PGE_2) and $PGF_{2\alpha}$ in the fracture callus of WT mice. **A,** Radiologic image of the bone fracture model in WT mice, produced by a transverse osteotomy that was stabilized with an intramedullary nail (**arrowhead**) at the midshaft of the right tibia at 8 weeks of age. **B,** Hematoxylin and eosin staining of the fracture callus 7 days after fracture (left), and immunohistochemical staining of mPGES-1 (middle and right). Boxed areas in the left panel are shown in higher magnification in the middle and right panels (left, bar = 1 mm; middle and right, bar = 100 μm). **C,** Time course (in days) of changes in mPGES-1, mPGES-2, and cytosolic PGES (cPGES) mRNA levels in the fracture callus of the right tibia and in the sham-operated site of the left tibia, determined by real-time reverse transcription–polymerase chain reaction. Bars show the mean ± SEM of 3 mice/group. * = $P < 0.05$ versus sham-operated site. **D,** PGE_2 and $PGF_{2\alpha}$ levels assessed by enzyme immunoassay in the fracture callus, as compared with the sham-operated site, at 7 days after surgery. Bars show the mean and SEM of 6 mice/group. * = $P < 0.01$ versus sham-operated site. See Figure 1 for other definitions.

per bone surface, and eroded surface per bone surface) (Figure 1F).

In addition to bone phenotypes, the height of the growth plate and the columnar architecture of chondrocytes were similar between the 2 genotypes (Figure 1E, bottom). This explains the observed lack of effect on skeletal growth, and indicates that the mPGES-1 deficiency does not affect chondrocyte function under normal physiologic conditions.

Skeletal phenotypes of mPGES-1$^{-/-}$ mice under pathophysiologic conditions. We then examined the effects of the mPGES-1 deficiency on bone phenotypes under pathophysiologic conditions. Initially, we investigated the involvement of mPGES-1 in bone loss induced by estrogen deficiency, by performing ovariectomy or sham operation on 26-week-old female mPGES-1$^{-/-}$ mice and their WT littermates. Four weeks after surgery, the change in BMD of the entire tibias of each mouse